J. Plasma Physics (2011), *vol.* 77, *part* 6, *pp.* 733–748. © Cambridge University Press 2011
doi:10.1017/S0022377811000158

Low-frequency fluctuations in scrape-off layer of tokamak plasma with limiter biasing

N. BISAI, RAMESWAR SINGH and R. SINGH

Institute for Plasma Research, Bhat, Gandhinagar 382 428, India
(rsingh129@yahoo.co.in)

(Received 3 February 2011, revised 15 March 2011 and acepted 21 March 2011;
first published online 26 April 2011)

Abstract. The effects of limiter biasing on the equilibrium density and potential profiles of the scrape-off layer (SOL) in tokamak plasma are investigated by including ionization and cross-field mobility. It is shown that a broadening of SOL can take place by the inclusion of ionization for low negative biasing. Various microinstabilities relevant for SOL plasmas have been studied. Generalized low-frequency dispersion relation is derived. It is shown that limiter biasing significantly modifies the SOL fluctuations. It is also shown that growth rate of conductive wall instability is smaller for negative biasing than positive biasing case. New mode, the modified Simon–Hoh, and ion temperature gradient instabilities are found to contribute significantly to the growth of curvature- and electron temperature-gradient-driven conductive wall instabilities.

1. Introduction

Physics of edge and scrape-off layer (SOL) tokamak plasma governs heat and particle deposition patterns on limiter or divertor plate, and first conducting wall of tokamak. Therefore, detailed physics knowledge in these regions is required to design these plates specifically for tokamak fusion reactor, where the heat and particle depositions are very intense. Various attempts have been made to know the SOL physics so that intensity of the particle and heat fluxes on the limiter/divertor can be minimized or controlled. A number of authors have investigated the problem experimentally as well as theoretically, but the shear complexity of the problem allows it to remain open. It has been established that spontaneous generation of radial electric field by biasing the electrode well inside the last closed magnetic flux surface (LCFS) can lead to interesting phenomena such as suppression of edge microturbulence leading to L-H transitions [1, 2], where L-H refers to low confinement to high confinement mode transitions. Turbulence stabilization has also been demonstrated by biasing a part of limiter surface in two-dimensional (2D) numerical simulation [3]. Limiter/divertor biasing experiments [4–7] have demonstrated that conventional density e-fold length, $\delta = (D_\perp L_\parallel / c_s)^{1/2}$ [where $D_\perp$ is the cross-field diffusion coefficient, $L_\parallel$ is the connection length, $c_s = (T_e/m_i)$, m_i is ion mass, and T_e is electron temperature], impurity concentration, and H_α lines can be significantly modified depending on the polarity of the biasing voltage between limiter/divertor plate and first conducting wall.

https://doi.org/10.1017/S0022377811000158 Published online by Cambridge University Press

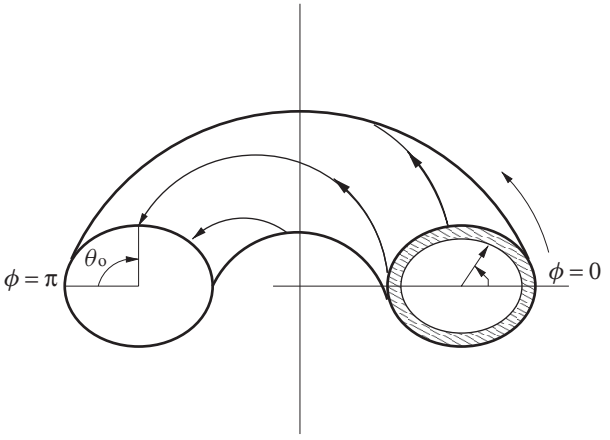


Figure 1. Tokamak geometry.

Earlier works by Nedospasov [8] and Berk et al. [9, 10] have brought out the significance of conducting wall instability (CWI) for SOL in tokamak plasma. It is shown that in the presence of conducting wall, the curvature-driven [8] and electron temperature gradient modes are unstable [9,10]. The underlying equilibrium in these cases was the one in which no net current was delivered to the limiter/divertor, which resulted in a simple relation between $\phi(x)$ and $T_e(x)$, that is, $\phi(x) = \ln \Lambda T_e(x)/e$, where $\Lambda = [m_i/4\pi m_e(1 + 1/\tau)]^{1/2}$ and $\tau = T_e/T_i$. Here x corresponds to radial coordinate. The model considered in Ref. [8] allows a local current (in poloidal angel θ) to flow to the limiter/divertor leading to θ_0-dependent equilibrium potential, where θ_0 is the middle of the arc line (see Fig. 1). Berk et al. have shown that the electron temperature gradient transverse to the magnetic field in plasma bounded by conducting walls gives rise to a rapid instability. They have pointed out that the instability can even develop in systems with straight field lines. On the basis of pressure, which is poloidally asymmetric and toroidally symmetric (due to fast diffusion along the toroidal direction), Rozhansky et al. [11] have shown a net radial current carried by ions, viz. $I = 2\pi R(P^- - p^+)/B$ (where I is the net radial current, $P^- - P^+$ is the pressure difference at the two end plates situated at the two poloidal locations, R is the major axis, and B is toroidal magnetic field), yields the cross-field ions mobility for the case of radially outward electric field. A recent work by Lachambre et al. [7] has described a simple equilibrium model, based on non-ambipolar radial transport [12,13] with an ion mobility as a free parameter and parallel sheath physics.

This paper is a detailed extension of earlier work presented in IAEA 1994 meeting by Charkrabarty et al. [14]. In this paper, first we have considered a new equilibrium in the presence of biased limiter using the effect of electron and ion mobilities and SOL ionization that can be controlled by gas puffing into the SOL. When limiter/divertor is negatively (positively) biased it collects only ions (electrons) flux. The limiter/diverter is situated at one toroidal location of the field lines so that it draws mainly in parallel direction. In our model, the parallel current drawn by limiter/diverter has been taken from the Bohm criterion. It is shown that the SOL equilibrium exists only when the electron (ion) has mobility in the range $3.75 \times 10^{-2} < \mu_\perp < 5.0 \times 10^{-1}$ for negatively (positively) biased limiter/divertor. Next, we have studied the stability of SOL plasma to well-known

https://doi.org/10.1017/S0022377811000158 Published online by Cambridge University Press

low-frequency perturbations. We have included the effect of the electron and ion temperature-gradient-driven CWIs [9, 10] modified by curvature effect and biasing limiter. We have also included contributions due to a modified Simon–Hoh instability (MSHI) [15, 16]. The physical mechanism of MSHI is quite similar to collisional Simon–Hoh (SH) and Rayleigh–Taylor instability in upper atmosphere and will be discussed latter. There exists a region of sharp variation of equilibrium electric field near to the LCFS. Such situation is very likely as the relative magnitude of parallel and perpendicular transports rapidly changes across the LCFS and specially during the improved confinement regime [17].

In brief, the purpose of the paper is twofold: (i) an equilibrium in the presence of biased limiter and ionization source in the SOL for constant electron temperature and zero ion temperature, and (ii) SOL low-frequency fluctuations due to curvature, modified Simon–Hoh, and ∇T_{e0}- and ∇T_{i0}-driven instabilities including the effect of biasing limiter.

The remainder paper is organized as follows. In Sec. 2, model equations describing SOL plasma are given. The SOL equilibrium of density and potential with biasing limiter has been described in Sec. 3. The local theory of conducting wall instabilities including ion temperature gradient, SH, and biasing effects are given in Sec. 4. In this section, we also have analyzed the dispersion relation and compared the growth rates for various CWI modes. Section 5 is devoted to conclusion and discussion.

2. Basic model equations

The SOL plasma is modeled by fluid description. The fluid model of the SOL plasma is justified since the parallel connection length of the field lines is typically much larger than mean free path of the plasma particles. The basic assumptions used for the model are quasi-neutrality of the plasma ($n_i = n_e = n$, where n_i and n_e refer to ion density and electron density of the plasma, respectively) and uniform ionization in the SOL.

The model equations used for the SOL plasma are electron continuity, ion continuity, current balance, electron energy, and ion energy equations. The equations are

$$\frac{\partial n}{\partial t} + \vec{\nabla} \cdot (n\vec{v}_e) = \gamma_{in} n, \tag{2.1}$$

$$\frac{\partial n}{\partial t} + \vec{\nabla} \cdot (n\vec{v}_i) = \gamma_{in} n, \tag{2.2}$$

$$\vec{\nabla} \cdot \vec{J} = 0, \tag{2.3}$$

$$\frac{3}{2} n \left(\frac{\partial}{\partial t} + \vec{v}_E \cdot \vec{\nabla} \right) T_e + p_e \vec{\nabla} \cdot \vec{v}_e = -\vec{\nabla} \cdot \vec{q}_e, \tag{2.4}$$

$$\frac{3}{2} n \left(\frac{\partial}{\partial t} + \vec{v}_E \cdot \vec{\nabla} \right) T_i + p_i \vec{\nabla} \cdot \vec{v}_i = -\vec{\nabla} \cdot \vec{q}_i, \tag{2.5}$$

where T_i, T_e, and γ_{in} are ion temperature, electron temperature, and gas ionization rate in the SOL, respectively. Terms $p_e \equiv nT_e$ and $p_i \equiv nT_i$ correspond to electron pressure and ion pressure, respectively. The symbol $\vec{J}$ represents total current due to electrons and ions, $\vec{J} = en\vec{v}_i - en\vec{v}_e$, where $\vec{v}_e$ and $\vec{v}_i$ refer to velocities of electrons and

https://doi.org/10.1017/S0022377811000158 Published online by Cambridge University Press

ions, respectively. These velocities can be written as $\vec{v}_e = \vec{v}_{\perp e} + \vec{v}_{\|e}$ and $\vec{v}_i = \vec{v}_{\perp i} + \vec{v}_{\|i}$. The symbols $\|$ and $\perp$ represent for parallel and perpendicular velocities of electrons and ions. The perpendicular velocities can be written as $\vec{v}_{\perp e} = \vec{v}_{eE} + \vec{v}_{\star e}$ and $\vec{v}_{\perp i} = \vec{v}_{iE} + \vec{v}_{\star i} + \vec{v}_{pi}$, where $\vec{v}_{eE} \equiv (\vec{E} \times \vec{B})/cB^2$, $\vec{v}_{\star e} \equiv -c(\vec{B} \times \vec{\nabla} p_e)/enB^2$, $\vec{v}_{iE} = -c\langle \vec{E} \rangle \times \vec{B}/B^2$, $\vec{v}_{\star i} \equiv c(\vec{B} \times \vec{\nabla} p_i)/enB^2$, and $\vec{v}_{pi} = (m_i c^2/eB^2)[\partial/\partial t + (\vec{v}_{\perp i} \cdot \vec{\nabla})]\vec{E}$; c and $\vec{E}$ represent velocity of light and electric field, respectively. The symbols $\vec{v}_{eE}$, $\vec{v}_{\star e}$, $\vec{v}_{iE}$, $\vec{v}_{\star i}$, and $\vec{v}_{pi}$ correspond to electron $\vec{E} \times \vec{B}$, electron diamagnetic, ion $\vec{E} \times \vec{B}$, ion diamagnetic, and ion polarization drifts, respectively. It is to be noted that ion $\vec{v}_{iE}$ drift term has $\langle \vec{E} \rangle$ term. The logic behind of it will be discussed in the next paragraph. The heat fluxes $\vec{q}_e$ and $\vec{q}_i$ correspond to electrons and ions, respectively. Explicit form of these can be found in standard Braginskii equations [18]. Heating and radiative power losses have been neglected.

Near the LCFS, the variation of equilibrium E is assumed to be so sharp that it varies significantly within one gyroradius. Therefore, if we consider a plane potential $\phi(x) = \phi \exp(ik_0 x)$, the ion responds to the gyro-orbit-averaged $E \times B$ drift as $\langle \vec{v}_E \rangle = (c/B^2)\vec{B} \times \vec{\nabla} \langle \phi(x) \rangle$, where $x = \bar{x} + a_i(\theta) = \bar{x} + a_i \cos(\theta)$, a_i is the ion Larmor radius, and k_0 is the inverse potential gradient scale length. By smoothing out the oscillating component, the gyro-averaged potential $\langle \phi \rangle$ can be expressed as

$$\langle \phi \rangle = \phi(\bar{x}) \frac{1}{2\pi} \int_0^{2\pi} d\theta \exp(ik_0 a_i \cos\theta) \simeq \left(1 - \frac{k_0^2 a_i^2}{4}\right) \phi(\bar{x}),$$

where $\phi(\bar{x})$ is averaged x-dependent potential, $k_0 = 1/L_\phi$, L_ϕ is potential scale length. This causes a relative $E \times B$ drift between electron and ion, which can be written as

$$\vec{v}_{eE} - \vec{v}_{iE} = (1/4) k_0^2 a_i^2 (c/B^2) \vec{E} \times \vec{B},$$

where $a_i = c_i/\Omega_i$ $c_i = (T_i/m_i)^{1/2}$ and $\Omega_i = eB/m_i c$. The symbol Ω_i refers to ion gyrofrequency.

In the SOL, the magnetic field lines intercept to the limiter/divertor, and the limiter/diverter collects ion (electron) current when the limiter/divertor is negatively (positively) biased with respect to the vacuum vessel. The total current enclosed to the limiter/divertor can be determined from Bohm sheath criterion. For Maxwellian plasma, expression of plasma current near the sheath is given by

$$J_\| = en \left[c_s (1 + 1/\tau)^{1/2} - \frac{c_e}{2\sqrt{\pi}} \exp\left[-\frac{e(\phi - \phi_L)}{T_e} \right] \right], \tag{2.6}$$

where $c_s = (T_e/m_i)^{1/2}$ and $c_e = (T_e/m_e)^{1/2}$ are electron thermal velocity and acoustic velocity, respectively. The parameters ϕ and ϕ_L are local potential and applied potential on the limiter, respectively.

3. Equilibrium with biasing

We investigate equilibrium in the presence of ionization source and biased limiter. We define equilibrium of a quantity f as $F = \langle f \rangle_y$ and $\partial F/\partial t = 0$, where $\langle f \rangle_y$ indicates poloidal (y) average of the f. Here, we assume that electrons and ions have diffusion ($D_\perp$) and mobility ($\mu_\perp$). It is to be noted these are phenomenological constants, not the usual transport coefficients (arising due to background turbulence). We further assume uniform T_e and $T_i = 0$ for simplicity of the problem, which indicate that we

https://doi.org/10.1017/S0022377811000158 Published online by Cambridge University Press

study only equilibrium of density and potential fields. The basic equations describing the equilibrium are ion and electron continuity equations, which are obtained from (2.1)–(2.2) using $N = \langle n \rangle_y$ and $\partial N/\partial t = 0$:

$$\vec{\nabla}_\perp \cdot (N\vec{v}_{\perp i}) + \nabla_\parallel (N v_{\parallel i}) = \gamma_{in} N, \tag{3.1}$$

$$\vec{\nabla}_\perp \cdot (N\vec{v}_{\perp e}) + \nabla_\parallel (N v_{\parallel e}) = \gamma_{in} N. \tag{3.2}$$

where $\vec{v}_{\perp i}$ and $\vec{v}_{\perp e}$ are the equilibrium ion and electron flow velocities. These can be obtained from ion and electron momentum equations, which are

$$v_{\perp i} = v_{iE} + v_{\star i} - D_{\perp i}\frac{\nabla N}{N} + \mu_{\perp i} E_\perp, \tag{3.3}$$

$$v_{\perp e} = v_{eE} + v_{\star e} - D_{\perp e}\frac{\nabla N}{N} - \mu_{\perp e} E_\perp. \tag{3.4}$$

First, we derive the generalized equation describing the SOL plasma when the limiter/diverter is negatively (positively) biased. In case the limiter/divertor is negatively (positively) biased, it collects only ions (electrons) current and plasma remains quasi-neutral (i.e. $\lambda_D \ll \delta$, where λ_D is the Debye length, δ is the width of the SOL), so that an equal amount of electrons (ions) current must flow to the wall. The one-dimensional (radial) equations describing the equilibrium are $\partial(J_{ex} + j_{ix})/\partial x = 0$ and $(\partial J_{ix}/\partial x)/eN = \gamma_{in}$ and using (2.6)–(3.4), we get

$$(D_{\perp i} - D_{\perp e})\frac{d^2 N}{dx^2} + \frac{d}{dx}\left(\mu_{\perp i} + \mu_{\perp e} N \frac{d\phi}{dx}\right) = \frac{N c_s}{L_\parallel}\left(1 - \sqrt{\frac{m_i}{4\pi m_e}} \exp\frac{-e[\phi - \phi_L]}{T_e}\right), \tag{3.5}$$

$$D_{\perp i}\frac{d^2 N}{dx^2} + \frac{d}{dx}\left(\mu_{\perp i} N \frac{d\phi}{dx}\right) = \frac{N c_s}{L_\parallel} - \gamma_{in} N. \tag{3.6}$$

Here, the integration along the field lines gives the $1/L_\parallel$ factor, where $L_\parallel$ is connection length. The second term in the right-hand side of (3.5) is smaller (greater) than one, if the limiter is negatively (positively) biased.

When we ignore the perpendicular mobility and ionization effects, the solution is

$$N \propto \exp(-x/\delta), \tag{3.7}$$

where $\delta = (D_{\perp i} L_\parallel / c_s)^{1/2}$ is the conventional e-folding length of SOL plasma and also is known as SOL width. If the limiter is floating, the plasma potential can be approximated by taking $J = 0$, which yields the relation between ϕ and T_e as $\phi = (T_e/e)\ln \Lambda$.

In our equilibrium model, we have not included the energy equations describing the SOL temperature gradients, which may have some dependence on the radiation losses, heating source (i.e, power input, RF source), and divergence of cross-field thermal flux. As the electron temperature is assumed constant, the exponential factor

https://doi.org/10.1017/S0022377811000158 Published online by Cambridge University Press

is independent of x. Combining (3.5)–(3.7), we get

$$\frac{d^2\bar{N}}{d^2\bar{x}} = k^2\bar{N}, \tag{3.8}$$

$$\frac{d}{dx}\left(\bar{N}\frac{d\bar{\phi}}{dx}\right) = \bar{N}\phi_0. \tag{3.9}$$

Here,

$$k = \left(\frac{c_s x_w^2 F(\mu)}{D^\star L_\parallel}\right)^{1/2},$$

$$\phi_0 = \left[\frac{c_s x_w^2 D_{\perp e} F(D)}{|\hat{\phi}_L|\mu_{\perp e} D^\star) L_\parallel}\right],$$

$$F(\mu) = 1 + \frac{\mu_{\perp i}}{\mu_{\perp e}} f(\hat{\phi}_L) - \left(1 + \frac{\mu_{\perp i}}{\mu_{\perp e}}\right)\hat{\gamma}_{in},$$

$$F(D) = 1 - \frac{D_{\perp i}}{D_{\perp e}} f(\hat{\phi}_L) - \left(1 - \frac{D_{\perp i}}{D_{\perp e}}\right)\hat{\gamma}_{in},$$

$$D^\star = 1 + \frac{D_{\perp e}\mu_{\perp e}}{D_{\perp i}\mu_{\perp i}},$$

$$f(\hat{\phi}_L) = \Lambda \exp(\hat{\phi}_L),$$

$\bar{N} = N/N_L$, $\hat{\phi}_L = e\phi_L/T_e$, $\hat{\gamma}_{in} = c_s\gamma_{in}/L_\parallel$, $\bar{\phi} = \phi/|\phi_L|$, $\bar{x} = x/x_w$, N_L and ϕ_L are averaged density and potential at the limiter, $x = 0$ is the limiter position, and x_w is the distance of wall from the inner edge of the limiter. We solve (3.8)–(3.9), analytically assuming parameters other than $\bar{\phi}$ and $\bar{N}$ are slowly varying function of $\bar{x}$ and using boundary conditions: (i) $\bar{x} \to 0$, $\bar{N} \to 1$, and $\bar{\phi} \to \pm 1$ (where +ve sign for positive biasing and –ve for negative biasing), (ii) $\bar{x} \to 1$, $\bar{N} \to N_w$, $\bar{\phi} \to 0$, $\bar{N} = \bar{N}_w$, and $\bar{\phi} \to 0$, where $\bar{N}_w = N_w/N_L$ and N_w is the plasma density at the wall. The solutions of (3.8)–(3.9) are

$$\bar{N} = \exp(kx) - A[\exp(kx) - \exp(-kx)], \tag{3.10}$$

$$\bar{\phi} = \frac{\phi_0}{k^2}\ln\left(\frac{\bar{N}}{\bar{N}_w}\right) + \left(\pm 1 + \frac{\phi_0}{k^2}\ln(\bar{N}_w)\right)F(A^\star). \tag{3.11}$$

Here the terms A and $F(A^\star)$ can be written as

$$A = (\exp(k) - \bar{N}_w)/(\exp(k) - \exp(-k)),$$

$$A^\star = \sqrt{(1-A)/A},$$

$$F(A^\star) = \frac{\tan^{-1}[A^\star \exp(kx)] - tan^{-1}[A^\star \exp(k)]}{\tan^{-1}(A^\star) - \tan^{-1}[A^\star \exp(k)]}.$$

We now estimate what must be the minimum value of $\mu_{\perp i}$ and $\mu_{\perp e}$ so that an equilibrium can arise. Let us consider the strong negative (positive) biasing limiter and assume that all electrons (ions) leaving the core plasma must go to the wall.

https://doi.org/10.1017/S0022377811000158 Published online by Cambridge University Press

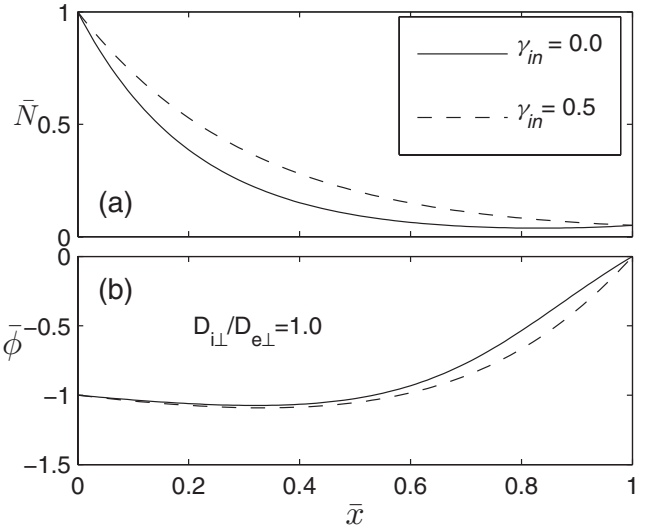


Figure 2. The density $\bar{N}$ and potential $\bar{\phi}$ as a function of $\bar{x}$ for two different values $\hat{\gamma}_{in}$. The other parameters are $\bar{N}_w = 0.05$, $x_w = 5.0$ cm, $D_{\perp i} = 10^4$ cm^2 s^{-1}, $e\phi_L/T_e = -10.0$, $\mu_{\perp i}/\mu_{\perp e} = 1.0$, and $D_{\perp i}/D_{\perp e} = 1.0$.

If $\mu_{\perp i}(\mu_{\perp e})$ for negative (positive) biasing is less than the minimum value, there will be accumulation of space charge and consequently the approximation of quasi-neutrality breaks down. In this case, the finite gyroradius effect is important. Therefore, this model can be applied to a case where ion gyroradius is much smaller than the radial gradient scale length. The minimum value of $\mu_{\perp i}(\mu_{\perp e})$ can be estimated as per following. Taking $\bar{N} \approx NAa$ total number of particles in a plasma (either ions or electrons), $A \approx (2\pi)^2 Ra$ is the surface area of the plasmas, a is the minor radius, R is the major radius, and N is the mean core plasma density, we can write $N/\tau_p A \approx N_s \mu_{\perp e} |d\phi/dr|$ for negatively biased limiter and $N/\tau_p A \approx N_s \mu_{i\perp} |d\phi/dr|$ for positively biased limiter. Here τ_p is the particle confinement time, x_w is the distance to the wall from inner edge of the limiter (LCFS), N_s is mean SOL plasma density, and ϕ is plasma density at LCFS. Employing $d\phi/dr \simeq \phi/x_w$, we get an estimate of the mobility as $\mu_\perp = Nax_w/\tau_p N_s \phi$. Thus, the upper limit on μ may be approximated from Einstein relation $\mu_\perp \approx eD_B/T_e$, where D_B is the Bohm diffusion coefficient. For typical SOL plasma parameters of ohmic heated tokamaks, $N/N_s \approx 3$, $T_i \approx T_e \approx 20\ eV$, the normalized plasma potential $e\phi/T_e \approx 5$, $x_w \approx 0.05$ m, $a \approx 0.25$ m, and $\tau_p \approx 10$ ms, we get the minimum value of $\mu_\perp = Nax_w/\tau_p N_s \phi \approx 0.0375$ m^2/V·s and the upper limit of $\mu_\perp \approx 0.5$ m^2/V·s for $D_B \approx 1$ m^2 s^{-1}. The physics of anomalous $\mu_\perp$ is similar to that $D_\perp$, i.e. the fluctuations scatter particles across B in such a way that they gain a finite velocity along $\nabla_\perp \phi$.

For negatively biased limiter, we plot the equilibrium plasma density and potential described by (3.10)–(3.11), for negatively biased limiter. Normalized plasma density ($\bar{N}$) and plasma potential ($\bar{\phi}$) versus normalized radial distance $\bar{x}$ are shown in Fig. 2 for different values of ionization rates $\gamma_{in} = 0.0$ and $\gamma_{in} = 0.5$. This shows that radial e-folding density and potential scale lengths increase by the inclusion of ionization effect. The other parameters used in this calculation are $\bar{N}_w = 0.05$, $x_w = 5$ cm,

https://doi.org/10.1017/S0022377811000158 Published online by Cambridge University Press

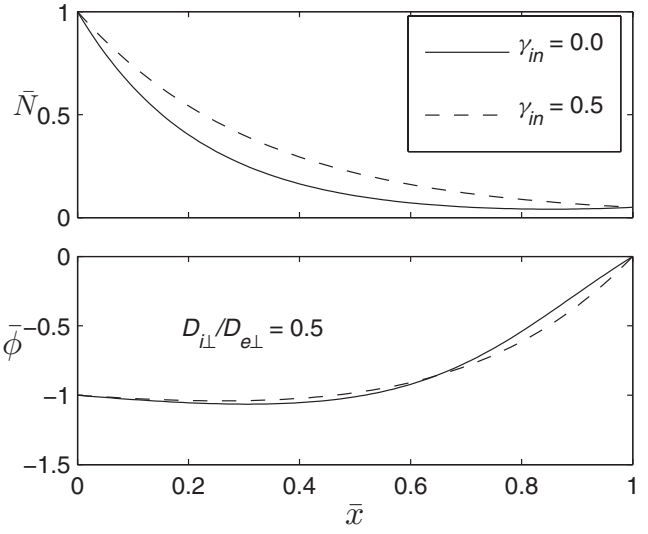


Figure 3. The density $\bar{N}$ and potential $\bar{\phi}$ variation with respect to $\bar{x}$ for different values of $\hat{\gamma}_{in}$. The other parameters are $\bar{N}_w = 0.05$, $x_w = 5.0$ cm, $D_{\perp i} = 10^4$ cm^2 s^{-1}, $e\phi_L/T_e = -10.0$, $\mu_{\perp i}/\mu_{\perp e} = 0.1$, and $D_{\perp i}/D_{\perp e} = 0.5$.

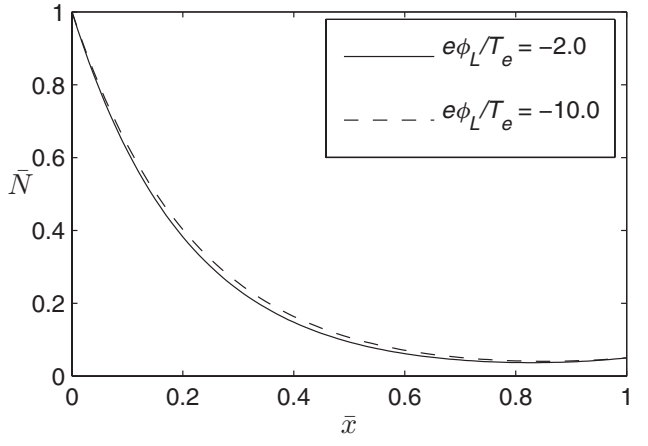


Figure 4. The density profile $\bar{N}(x)$ as a function of $\bar{x}$ for limiter biased at potential $e\phi_L/T_e = -2.0, -10.0$. The other parameters are $\bar{N}_w = 0.05$, $x_w = 5.0$ cm, $D_{\perp i} = 10^4$ cm^2/s, $\mu_{\perp i}/\mu_{\perp e} = 0.1$, and $D_{\perp i}/D_{\perp e} = 1.0$.

$D_{\perp i} = 10^4$ cm^2 s^{-1}, $\mu_{\perp i}/\mu_{\perp e} = 0.1$, $e\phi_L/T_e = -10.0$, and $D_{\perp i}/D_{\perp e} = 1.0$. The plasma density ($\bar{N}$) and potential ($\bar{\phi}$) as a function of $\bar{x}$ for $D_{\perp i}/D_{\perp e} = 0.5$ is shown in Fig. 3. The spread of SOL can be physically explained as the ionization source effectively enhances the parallel loss time and hence extra space charge accumulates in the SOL. The accumulations of extra space charge are responsible to spread out the SOL. For $\bar{N}_w = 0.05$, $x_w = 5$ cm, $D_i = 10^4$ cm^2 s^{-1}, $\mu_{\perp i}/\mu_{\perp e} = 0.1$, and $D_{\perp i}/D_{\perp e} = 1.0$, the plot of $\bar{N}$ with respect to $\bar{x}$ is shown in Fig. 4 for $e\phi_L/T_e = -2$

https://doi.org/10.1017/S0022377811000158 Published online by Cambridge University Press

(solid curve) $e\phi_L/T_e = -10$ (dashed curve). Figure 4 shows that the normalized e-folding length increases for high negative potential biasing. The shortcoming of our simple model is that it is inadequate to describe the equilibrium profiles for positive biased limiter. It is because of the fact that when the limiter bias approaches to zero or higher positive potential, then the right-hand side second term of (2.6) is not valid. However, LaBombard et al. [12,13] have used an approximation by setting electron flux to the random flux and ions to Nc_s and have estimated the effect of limiter positive biasing. For simulating the positive as well as negative biasing case, the problem should be treated as 2D with full nonlinear terms. Next, we study the posible low-frequency ($\omega < \Omega_i$) instabilities in plasma with open field lines.

4. Linear instability analysis

We study the stability of SOL to well-known low-frequency ($\omega < \Omega_i$) microinstabilities, namely electron temperature-gradient/curvature-driven CWI. We also include contribution due to a gyro-averaged electric field (MSHI effect), ion temperature gradient, finite mobility of electrons and ions, and limiter biasing on these phenomena. The MSHI effect arises due a sharp variation of equilibrium DC electric field over a region near the last closed flux surface.

The expression for equilibrium plasma current to the limiter is given by sheath physics by (2.6). The current balance equation can be written as

$$\vec{\nabla}_\perp \cdot (en\vec{v}_{\perp i} - en\vec{v}_{\perp e}) = -\nabla_\parallel J_\parallel. \tag{4.1}$$

For simplicity, we have neglected the effects of diffusion in the instability analysis. The basic equations for low-frequency fluctuations are given in Sec. 2. The governing equations are (i) vorticity equation ($\vec{\nabla} \cdot \vec{J} = 0$), (ii) plasma current drawn into limiter, (iii) electron continuity equation, and (iv) electron energy equation and ion energy equation [19]. These equations after linearizing can be written as

$$a_s^2 \left(\frac{\partial}{\partial t} + \vec{v}_E \cdot \vec{\nabla} + \vec{v}_{\star i} \cdot \vec{\nabla} \right) \nabla_\perp^2 \tilde{\phi} + \epsilon_n v_{\star n} \cos\theta \frac{\partial}{\partial y} [\tilde{n}(1 + 1/\tau) + \tilde{t}_e + \tilde{t}_i/\tau]$$

$$+ \frac{k_0^2 a_i^2}{4} v_{Ex} \frac{\partial \tilde{n}}{\partial y} = \frac{\partial}{\partial s} \left(\frac{\tilde{J}_\parallel}{eN} \right), \tag{4.2}$$

$$\tilde{J}_\parallel = \left[\tilde{n} + \frac{1}{2} \frac{\tau}{\tau + 1} (\tilde{t}_e + \tau^{-1} \tilde{t}_i) \right] J_{\parallel 0} + \frac{eNc_e}{4\sqrt{\pi}} \left[\frac{1}{1+\tau} \tilde{t}_i \right] \exp\left[-e \frac{\phi - \phi_L}{T_e} \right]$$

$$+ \frac{eNc_e}{2\sqrt{\pi}} \left(\tilde{\phi} - \left[\frac{e(\phi - \phi_L)}{T_e} + \frac{1}{2} - \frac{1}{2} \frac{\tau}{1+\tau} \right] \tilde{t}_e \right) \exp\left(\frac{-e[\phi - \phi_L]}{T_e} \right), \tag{4.3}$$

$$\left(\frac{\partial}{\partial t} + \vec{v}_E \cdot \vec{\nabla} \right) \tilde{n} + v_{\star n} \frac{\partial \tilde{\phi}}{\partial y} = 0, \tag{4.4}$$

$$\left(\frac{\partial}{\partial t} + \vec{v}_E \cdot \vec{\nabla} \right) \tilde{t}_e + \eta_e v_{\star n} \frac{\partial \tilde{\phi}}{\partial y} = 0, \tag{4.5}$$

$$\left(\frac{\partial}{\partial t} + \vec{v}_E \cdot \vec{\nabla} \right) \tilde{t}_i + \eta_i v_{\star n} \frac{\partial \tilde{\phi}}{\partial y} = 0. \tag{4.6}$$

https://doi.org/10.1017/S0022377811000158 Published online by Cambridge University Press

Here perturbed quantities are indicated by a customary over tilde symbol: $\tilde{n} = n/N$, $\tilde{\phi} = e\phi/T_e$, $\tilde{t}_e = t_e/T_i$, $\tilde{t}_i = t_i/T_i$, $\epsilon_n = 2L_n/R$, $a_s = c_s/\Omega_i$, $v_{\star n} = a_s c_s/L_n$, $L_n = (-d\ln N/dx)^{-1}$, $v_{\star i} = -(1+\eta_i)(T_i/T_e)v_{\star n}$, $\eta_e = L_n/L_{T_e}$, $\eta_i = L_n/L_{T_i}$, $L_{T_j} = (-d\ln T_j/dx)^{-1}$. We also assume that fluctuation is smaller than the density gradient scale length (i.e. $k_x L_n >> 1$) and $\vec{E}\times\vec{B}$ convection dominates in ion and electron energy equations. Using Fourier transform and integrating along the field, we get the generalized dispersion relation

$$k_\perp^2 a_s^2 \bar{\omega}(\bar{\omega} + \tau^{-1}\omega_{\star n}(1+\eta_i)) + \epsilon_n \frac{q}{\pi}\omega_{\star n}^2(1+\eta_e+1/\tau+\eta_i/\tau)\sin(\pi/q)\cos\theta_0$$

$$+\frac{k_0^2 a_s^2}{4}\omega_E\omega_{\star n} = -i\omega_{\star n}\left[1+\frac{1}{2}\frac{\tau}{1+\tau}(\eta_e+\tau^{-1}\eta_i)\right]\frac{1}{2\pi R}\frac{J_{\parallel 0}}{eN} - i\frac{c_e}{4\pi^{3/2}R}$$

$$\times\left[\bar{\omega} - \eta_e\omega_{\star n}[e(\phi-\phi_L)/T_e + 1/2] + \tfrac{\omega_{\star n}}{2}(\eta_e+\tau^{-1}\eta_i)\tfrac{\tau}{1+\tau}\right]\exp\left(-\tfrac{e[\phi-\phi_L]}{T_e}\right) \qquad (4.7)$$

where, $\bar{\omega} = \omega - \omega_E$, $\omega_E = k_y v_E$, $\omega_\star = k_y v_{\star n}$, $ds = qRd\theta$, $(\theta_1+\theta_2)/2 = \theta_0$ is the middle arc of the field lines as is shown in Fig. 1, $\theta_2 - \theta_1 = 2\pi/q$, $q = aB_\phi/RB_\theta$, and B_ϕ and B_θ are the toroidal and poloidal magnetic field strength, respectively. It is to be noted that we have linearized sheath current and variation of the parallel current is taken as $\partial\tilde{J}_\parallel/\partial s = \tilde{J}_\parallel/2\pi R$ in (4.7). This is normally true for SOL region where magnetic field lines are opened to the limiter and parallel dynamics is determined by the sheath physics. We have neglected effect of magnetic shear. Normally, the shear is resposible stabilization of small k_y modes. The sheath conductivity also stabilizes the small k_y modes in SOL [10, 20, 21]. Sarazin et al. in Ref. [20] accommodated this stabilization effect of the magnetic shear indirectly including higher sheath conduction current than the current obtained from purely sheath physics as the effect of sheath current and magnetic shear is similar. Detailed theoretical discussion about the magnetic shear can be found in Refs [10, 22]. In the absence of ion temperature perturbation and SH effects, (4.7) yields the same dispersion relation as is given in Ref. [14]. Here the second term corresponds to the local current in θ to flow to the limiter, where the poloidal variation of equilibrium is assumed to be small. When the limiter is floating, the values of $e\phi_0/T_e$ and $J_{\parallel 0}/eN$ for typical SOL parameters are $e\phi_0/T_e = 2.8$ and $J_{\parallel 0}/eN \simeq 3.7\times 10^6$ cm s^{-1}.

4.1. *Temperature-gradient-driven conducting wall instability*

In the absence of density gradient ($\omega_{\star n} = 0$) and curvature ($\epsilon_n = 0$) effects, the effect of temperature-gradient-driven CWIs can readily recover from (4.7). In that case, the dispersion relation of ∇T_e- and ∇T_i-driven CWI is given by

$$k_\perp^2 a_s^2 \bar{\omega}^2 = -i\frac{c_e}{4\pi^{3/2}R}\left(\frac{1}{2}\frac{\tau}{1+\tau}\omega_{\star n}(\eta_e+\tau^{-1}\eta_i)\right)\exp\left[-\frac{e(\phi-\phi_L)}{T_e}\right]$$

$$-i\frac{c_e}{4\pi^{3/2}R}\left(\bar{\omega} - \eta_e\omega_{\star n}\left[\frac{e(\phi-\phi_L)}{T_e}+\frac{1}{2}\right]\right)\exp\left(-\frac{e(\phi-\phi_L)}{T_e}\right). \qquad (4.8)$$

Here, the first term of right-hand side of (4.8) is formed through perturbations in parallel ion current, i.e. $J_{\parallel i} = en[(T_e+T_i)/m_i]^{1/2}$, and the parallel current perturbation

https://doi.org/10.1017/S0022377811000158 Published online by Cambridge University Press

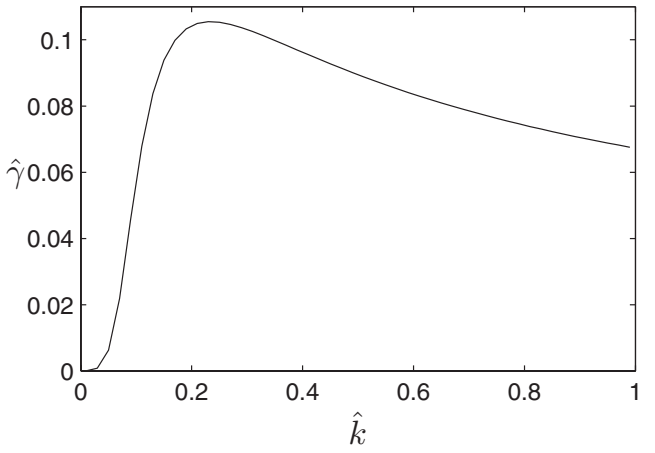


Figure 5. Plot of growth rate $\hat{\gamma}(=\gamma L_n/c_s)$ versus $\hat{k}(=k_\perp a_s)$ for parameters $\eta_e=\eta_i=\tau=1$, $\hat{\gamma}_{in}=0$, $L_n=2.0$ cm, $R=100.0$ cm, $T_e=10$ eV, and floating limiter.

yields the second term in the right-hand side as earlier derived by Berk et al. [9]. For homogeneous ion temperature gradient ($\nabla T_{i0}=0$) in SOL and $\eta_e\omega_{\star n}>\omega$, the frequency and growth rate of ∇T_{e0}–driven CWI, when the limiter is floating can be given by

$$\bar{\omega}=\frac{1}{\sqrt{2}}(1+i)\left[\frac{c_e\eta_e\omega_{\star n}}{8\pi^{3/2}Rk_\perp^2a_s^2\Lambda}\left(2\ln\Lambda+1-\frac{\tau}{1+\tau}\right)\right]^{1/2}$$

$$\simeq\frac{1}{2\sqrt{2}}(1+i)\left(\frac{c_s^2}{\pi RL_{T_e}k_\perp a_s}\right)^{1/2}\left(2\ln\Lambda+1-\frac{\tau}{1+\tau}\right)^{1/2}\left(\frac{1+\tau}{\tau}\right)^{1/4}. \quad (4.9)$$

For $\tau>1$, the frequency and growth of ∇T_{e0}–driven CWI is similar to earlier given in Refs [8,9]. For homogeneous electron temperature in the SOL, the $\eta_i\omega_{\star n}>\omega$, the ion temperature gradient conductive wall instability survives with real frequency and growth rate,

$$\bar{\omega}=\frac{1}{2}(-1+i)\left[\frac{c_e\eta_i\omega_{\star n}}{8\pi^{3/2}Rk_\perp^2a_s^2\Lambda}\frac{1}{1+\tau}\right]^{1/2}$$

$$\simeq\frac{1}{2\sqrt{2}}(-1+i)\left(\frac{c_s^2}{\pi RL_{T_i}k_\perp a_s}\right)^{1/2}\left(\frac{1}{\tau(1+\tau)}\right)^{1/4}. \quad (4.10)$$

It is to be noted that the magnitude of growth of both the instabilities is the same order, but they propagate poloidally opposite to each other.

We now study the combined effect of electron and ion temperature-gradient-driven conductive wall instabilities by plotting (4.8). The normalized growth rate $\hat{\gamma}(=\gamma L_n/c_s)$ as a function of $\hat{k}(=k_\perp a_s)$ is given in Fig. 5 for floating limiter. The growth rate changes with $\hat{k}$ and has maximal at $k_\perp a_s\sim 0.2$ for parameters $\eta_e=\eta_i=\tau=1$. In Fig. 6, the growth rates as a function of η_i for various η_e are shown. This depicts the strong effect of ∇T_{e0} on ∇T_{i0}–driven CWI. The growth rate

https://doi.org/10.1017/S0022377811000158 Published online by Cambridge University Press

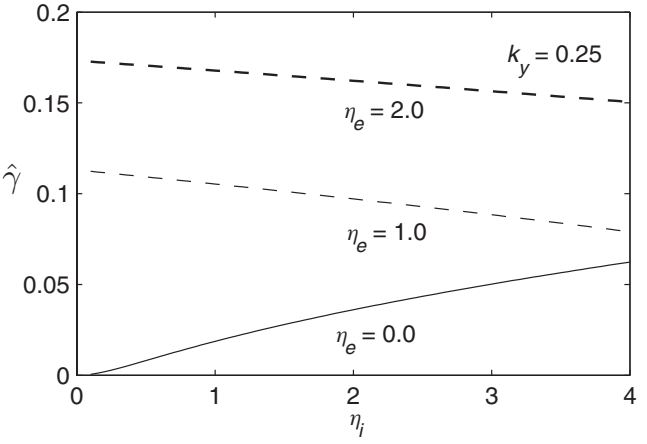


Figure 6. Plot of growth rate ($\hat{\gamma}$) as function of η_i is shown for various values of η_e and without biasing. The other parameters are $\hat{k} = 0.025$, $\tau = 1$, $\hat{\gamma}_{in} = 0$, $L_n = 2.0$ cm, $R = 100.0$ cm, and $T_e = 10$ eV.

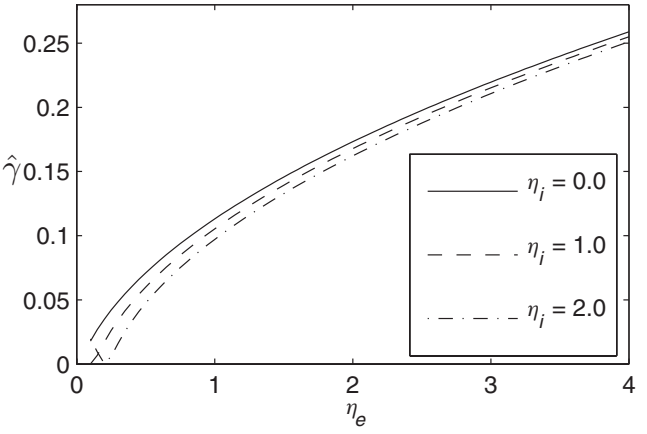


Figure 7. The growth rate ($\hat{\gamma}$) as function of η_e for various η_i without biasing. The other parameters are $\hat{k} = 0.025$, $\tau = 1$, $\hat{\gamma}_{in} = 0$, $L_n = 2.0$ cm, $R = 100.0$ cm, and $T_e = 10$ eV.

versus η_e for various η_i is shown in Fig. 7. The ion temperature gradient (η_i) has the weak effect on ∇T_{e0}–driven CWI. Finally, the effect of biasing including temperature gradient modes is shown in Fig. 8. This shows suppression of fluctuations for both negative and positive biasing.

4.2. Curvature and modified Simon–Hoh instabilities

In the limit when the limiter is floating, and $\nabla T_{e0} = 0$ and $\nabla T_{i0} = 0$, equating $\bar{\omega} \exp[-e(\phi - \phi_L)/T_e]$ term on the right-hand side of (4.7) with $\cos\theta_0$ term and $k_0^2 a_i^2$ term corresponds to MSHI on left-hand side, we can recover the purely growing

https://doi.org/10.1017/S0022377811000158 Published online by Cambridge University Press

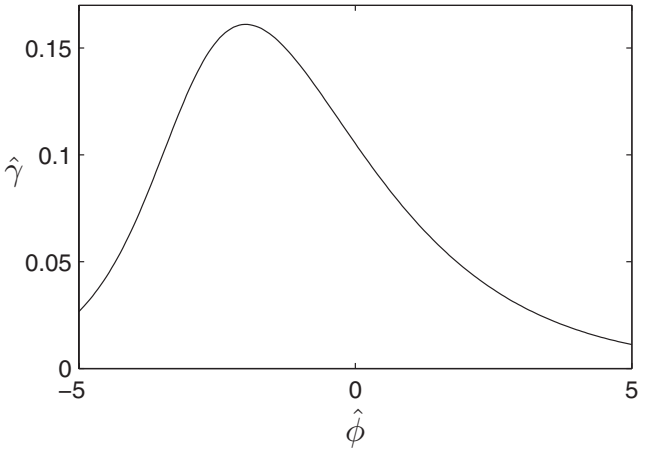


Figure 8. The growth rate ($\hat{\gamma}$) as function of biasing potential $\hat{\phi}(= e\phi_L/T_e)$ for fixed values of $\hat{k} = 0.025$, $\eta_e = \eta_i = \tau = 1$, $\hat{\gamma}_{in} = 0$, $L_n = 2.0$ cm, $R = 100.0$ cm, and $T_e = 10$ eV.

curvature-driven mode as earlier derived in Ref. [8]. The growth rate is given by

$$\gamma = 4qk_\perp a_s \omega_{\star n} \left(\frac{\tau}{1+\tau}\right)^{1/2} \sin(\pi/q)\cos\theta_0 + \pi R k_\perp \omega_{\star n} \left(\frac{\tau}{1+\tau}\right)^{1/2} \left(k_0^2 a_s^2 \frac{v_{E\times B}}{c_s}\right). \tag{4.11}$$

This is simplified form of curvature-driven CWI with MSH effect. The above dispersion relation is valid only when the mode wavevector satisfies the condition $k_\perp a_s < (L_n/8\pi qR)^{1/4}$. The second term in the right-hand side of (4.11) is corresponding to ion gyro-averaged $\vec{E}\times\vec{B}$ drift effect also known as MSH effect [15]. The instability mechanism due to finite ion gyro-averaged effect may be best understood as: due to large Larmor radius the ions with their guiding center at maximum electric field spend most of their time in low E region than electrons. In such a case, the gyro-averaged $\vec{E}\times\vec{B}$ drift velocity for ion is smaller than electrons. The effect leads to current in the $\vec{E}\times\vec{B}$ direction, viz. $\vec{v}_{eE} - \vec{v}_{iE} = (1/4)k_0^2 a_i^2 c(\vec{E}\times\vec{B})/B^2$ and causes charge separation and density perturbation in poloidal direction and, as a result, it produces a perturbed poloidal electric field (δE_θ). The $\delta\vec{E}_\theta \times \vec{B}$ enhances the density perturbations only if $\vec{E}_0 \cdot \vec{\nabla} N_0 > 0$.

In the similar long wavelength (i.e. $k_\perp a_s < (L_n/8\pi qR)^{1/4}$) limit, and if temperature gradients are finite, the unstable curvature–MSH-driven CWI owns real frequency that is $\omega_r > \gamma$. The frequency and growth is given by

$$\omega_r + i\gamma = \eta_e \omega_{\star n}\left[\ln\Lambda + \frac{1}{2} - \frac{1}{2}\frac{\tau}{1+\tau}\right] - \frac{1}{2}\tau\eta_i\omega_{\star n}\left(\frac{\tau}{1+\tau}\right) + i4qk_\perp a_s\omega_{\star n}\left(\frac{1+\tau}{\tau}\right)^{1/2}$$
$$\times \sin(\pi/q)\cos\theta_0 + i\pi R k_\perp \omega_{\star n}\left(\frac{1+\tau}{\tau}\right)^{1/2}\left(k_0^2 a_s^2 \frac{v_{E\times B}}{c_s}\right). \tag{4.12}$$

https://doi.org/10.1017/S0022377811000158 Published online by Cambridge University Press

When the limiter is biased, the growth of curvature–MSH-driven CWI instability, including temperature gradient effect, can be written as

$$\gamma = \frac{4\pi^{3/2}R}{c_e}\left[\epsilon_n \frac{q}{\pi}\omega_{\star n}^2(1+\eta_e+1/\tau+\eta_i/\tau)\sin(\pi/q)cos\theta_0 + \frac{k_\perp^2 a_i^2}{4}\omega_E\omega_{\star n}\right]$$

$$\exp\left(\frac{e}{T_e}(\phi-\phi_L)\right). \tag{4.13}$$

It is evident from (4.13) that growth rate of curvature-CWI increases with increasing electron and ion temperature gradients. Also it is to be noted that when limiter/diverter is negatively biased with respect to the wall, the growth rate of this mode significantly enhances than positively biased limiter case. We also observe that the growth rate of temperature-gradient-driven CWI is a weaker instability than driven CWI. This can radially be shown that comparing the growths from (4.9) and (4.11), which yields the relation $(L_n^2/\pi R L_T)^{1/2} \leqslant 8\sqrt{2}q(k_\perp a_s)^{5/2}$. This inequality can easily satisfy for typical SOL plasma parameters $L_n = L_T = 2$ cm, $R = 100$ cm, $q \geqslant 3.5$, and $k_s a_s \simeq 0.2$.

4.3. Interchange mode

Interchange mode, which is unaffected by open field lines physics (i.e. sheath effects), is another strong candidate among modes studied above for driving turbulence in the SOL plasmas. This mode has significant growth but has a narrow band in $k_\perp$ space. The sheath effect can be ignored for shorter scale interchange modes if

$$k_\perp a_s > \frac{1}{8q}\left(\frac{\tau}{1+\tau}\right)^{1/2}\frac{\ln \Lambda}{\sin(\pi/q)\cos\theta_0}. \tag{4.14}$$

The lower boundary of the mode in $k_\perp$ space is determined by the finite Larmor radius effect. For $L_n = L_{Te} = L_{Ti}$, $\eta_e = \eta_i = \eta$, the $k_\perp$ space spectrum boundary for strongly growing interchange mode given by

$$\left[\tau(1+\tau)\frac{8qL_n}{\pi R}\frac{1+2\eta}{(1+\eta)^2}\right]^{1/2} > k_\perp a_s > \frac{1}{8q}\left(\frac{\tau}{1+\tau}\right)^{1/2}\frac{\ln \Lambda}{\sin(\pi/q)\cos\theta_0}. \tag{4.15}$$

For above limiting case, the growth of interchange can be written as

$$\gamma \simeq \sqrt{\frac{2qc_s^2}{\pi R L_n}\left(1+\frac{1}{\tau}+\eta_e+\frac{\eta_i}{\tau}\right)\left(\sin(\pi/q)\cos\theta_0\right)}. \tag{4.16}$$

In the same limiting case, the growth rate of MSH instability is given by

$$\gamma = \frac{c_s}{L_\phi}\sqrt{\frac{a_s v_{E\times B}}{L_n c_s}}. \tag{4.17}$$

Here, L_ϕ is potential scale length in SOL.

4.4. Comparison of different growth rates

The generalized dispersion relation (4.7) is used to compare growth rates of different modes. The normalized growth rate $\hat{\gamma}$ versus k_y is shown in Fig. 9 in the case of zero biasing. The solid line indicates the plot of generalized dispersion relation including all modes, namely, magnetic curvature, SH, and ∇T_e- and ∇T_i-driven CWI instabilities. The dotted line represents the growth in the absence of curvature

https://doi.org/10.1017/S0022377811000158 Published online by Cambridge University Press

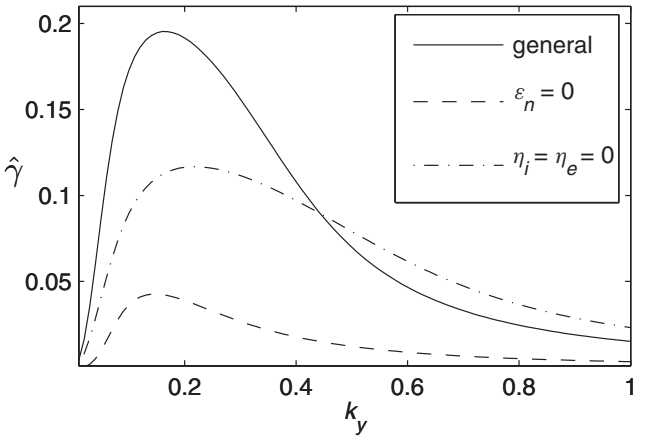


Figure 9. The growth rate ($\hat{\gamma}$) as function of $\hat{k}$ for no biasing. The solid line represents the plot of generalized dispersion relation, (4.7), the dashed line is corresponding to growth without curvature–SH effects ($\epsilon_n = 0$), the dashed dotted line stands for ($\epsilon_n \neq 0$) and $\eta_i = \eta_e = 0$. Parameters $\hat{k} = 0.025$, $\tau = 1$, $\hat{\gamma}_{in} = 0$, $L_n = 2.0$ cm, $R = 100.0$ cm, $B = 0.8$T, and $T_e = 10$ eV are used when these are necessary.

($\epsilon_n = 0$) effect where the other parameters are taken as $\eta_i = \eta_e = \tau = 1$. This shows that the growth rate of instability reduces considerably in the absence of curvature. Dashed dotted line shows the growth rate for parameters $\eta_e = \eta_i = 0$, $\tau = 1$, $\epsilon_n \neq 0$. This implies that both curvature- and temperature-gradient-driven CWIs play crucial role in driving turbulence in SOL of tokamak plasmas.

5. Conclusion

We have analyzed SOL equilibrium in the presence of biased limiter and controlling ionization rates by gas puffing. It is observed that the equilibrium radial density profile and potential profile are broaden in the SOL by the inclusion of ionization. It happens as the ionization source effectively enhances the parallel loss time. The SOL equilibrium profiles exist when electron (ion) mobility has a range $3.75 \times 10^{-2} < \mu_\perp < 5.0 \times 10^{-1}$ for negative (positive) biasing. The stability of SOL to low-frequency perturbations of electron temperature-gradient-driven, ion temperature-gradient-driven, curvature-driven, and MSHI-driven modes in the presence of biased limiter has been analyzed. The MSHI, which arises because of relative drift between electron and ion near the LCFS, modifies the growth rate of curvature-driven instabilities. It is shown that even for flat electron temperature profile (or in the absence of standard electron temperature-gradient-driven CWI), the ion temperature-gradient-driven conductive wall mode survives. The suppression of temperature-gradient-driven instabilities is found for both negative and positive biasing. We also observed that the growth rate of temperature-gradient-driven CWI is a weaker instability than the curvature-driven CWI if the inequality $(L_n^2/\pi R L_T)^{1/2} \leqslant 8\sqrt{2}q(k_\perp a_s)^{5/2}$ is satisfied in the SOL. We have also found that the growth rate of conductive wall instability is smaller for negative biasing limiter/divertor with respect to the wall than for positive biasing case. Most destabilizing effect is seen when the limiter/divertor is slightly negative with respect to the wall.

https://doi.org/10.1017/S0022377811000158 Published online by Cambridge University Press

References

[1] Tayor, J. B., Brown, M. L., Fried, B. D. and Grate, H. 1989 *Phys. Rev. Lett*. **63**, 2365.
[2] Wagner, F., Becker, G., Behringer, K. and Campbell, D. 1982 *Phys. Rev. Lett*. **49**, 1408.
[3] Ghendrih, Ph., Sarazin, Y., Attuel, G. et al. 2003 *Nucl. Fusion* **43**, 1013.
[4] Shoji, T., Aikawa, H., Annaratone, B. M. et al. 1993 Divertor bisas experiment on JET-2M. In: *Proc. Fourteenth Int. Conf. Plasma Physics and Controlled Nuclear Fusion Research, Würzburg, Germany, 30 September–7 October 1992*, vol. 1 (ed. Editorial staff of IAEA). Plasma Physics and Controlled Nuclear Fusion Research 1992, IAEA-CN-56/A-5-5, pp. 323–327.
[5] Takamura, S., Kinoshita, S. and Uesugi, Y. 1991 *IEEE* **19**, 885.
[6] Phillips, P. E., Wooten, A. J., Rowan, R. W., Ritz, C. P. et al. 1987 *J. Nucl. Mater*. **145–147**, 807.
[7] Lachambre, J. L., Quirion, B., Boucher, C., Decoste, R. et al. 1994 *Nucl. Fusion* **34**, 1431.
[8] Nedospasov, V. 1989 *Sov. J. Plasma Phys*. **15**, 659.
[9] Berk, H. L., Ryutov, D. D. and Tsidulko, Yu. 1991 *Phys. Fluids* **B3**, 1346.
[10] Berk, H. L., Cohen, R. H., Ryutov, D. D., Tsidulko, Yu. A. and Xu, X. Q. 1993 *Nucl. Fusion* **33**, 263.
[11] Rozhansky, V. and Tendler, M. 1994 *Phys. Plasmas* **1**, 2711.
[12] LaBombard, R. W. C. and Tynan, G. 1990 *Plasma. Phys. Contr. Fusion* **32**, 383.
[13] LaBombard, B. 1990 *Nucl. Fusion* **30**, 485.
[14] Chakrabarti, N., Das, A., Deshpande, S., Kaw, P. K., Mahajan, S., Sen, A. and Singh, R. 1995 Physics of SOL/EDGE Turbulence Phenomena in tokamaks. In: *Proc. Fifteenth Int. Conf. Plasma Physics and Controlled Nuclear Fusion Research, Seville, Spain, 26 September–1 October 1994*, vol. 3 (ed. Editorial Staff of IAEA). Plasma Physics and Controlled Nuclear Fusion Research 1994, IAEA-CN-60/D-9, pp. 289–298.
[15] Sakawa, Y., Joshi, C., Kaw, P. K., Chen, F. F. and Jain, V. K. 1993 *Phys. Fluids* B **5**, 1681.
[16] Jacob, S., Jain, K. K., Mahajan, S., Saxena, Y. C., Sen, A. K. and Singh, R. 1995 Fluctuation supression by bias electrod induced poloidal flow and feedback in a toroidal plasma. In: *Proc. Fifteenth Int. Conf. Plasma Physics and Controlled Nuclear Fusion Research, Seville, Spain, 26 September–1 October 1994*, vol. 2 (ed. Editorial Staff of IAEA). Plasma Physics and Controlled Nuclear Fusion Research 1994, IAEA-CN-60/A3/A5-P16, pp. 295–302.
[17] Hazeltine, R. D., Xiao, H. and Valanju, P. M. 1993 *Phys. Fluids* B **5**, 4011.
[18] Braginskii, S. I. 1965 *Review of Plasma Physics*, Vol. 1. New York: Consultant Bureau.
[19] Singh, R., Kaw, P. K. and Mahajan, S. 1996 *Plasma. Phys. Contr. Fusion* **38**, 1985.
[20] Sarazin, Y. and Ghendrih, Ph. 1998 *Phys. Plasmas* **5**, 4214.
[21] Bisai, N., Das, A., Deshpande, S., Jha, R., Kaw. P., Sen, A. and Singh. R. 2004 *Phys. Plasmas* **11**, 4018.
[22] Garbet, X., Laurent, L., Roubin, J.-P. and Samain, A. 1991 *Nucl. Fusion* **31**, 967.

https://doi.org/10.1017/S0022377811000158 Published online by Cambridge University Press